Generalized RF Time Domain Imaging Technique for Moving Objects on Conveyor Belts in Real Time

Zubair Akhter, *Student Member*, *IEEE*, Abhishek Kumar Jha, *Member*, *IEEE* and M. Jaleel Akhtar, *Senior Member*, *IEEE*

***Abstract*— In this paper, an attractive time domain RF imaging technique is proposed for online monitoring of moving objects over conveyor belts. The proposed technique combines the strength of the time domain approach and the Riccati equation based ultra-wide band reconstruction method in order to image the stratified lossy dielectric medium. The applicability of the proposed method is first tested under stationary condition by reconstructing the permittivity and conductivity image of the target area comprising of various standard samples placed in free space. For moving objects under real world scenario, two antenna arrays comprised of UWB Vivaldi elements are designed and tested. These arrays are then employed to produce the 2-D microwave image of various wooden based samples and human mannequins carrying metal object concealed behind the cloth. The obtained real time microwave image of the test medium shows that the proposed RF imaging technique is best suited for online monitoring of stationary as well as moving targets, where the structural as well as the electrical properties of the test medium can be obtained through a nondestructive process without using any iterative scheme.**

Keywords— Microwave imaging; nondestructive evaluation; online contraband detection; time domain technique.

I. INTRODUCTION

The development of low cost, less complex RF/microwave imaging techniques for various industrial applications has attracted lot of interest by various research groups in recent years. The focus is more on developing non-iterative techniques so that they can be applied for real time applications. The RF time domain measurement technique provides the platform for the researcher to develop cost effective procedure for imaging and material testing [1]-[15]. The time domain method employs a simple calibration scheme, and hence the complex calibration procedures of the frequency domain approach can be avoided. In the past, a number of time domain techniques based on simple calibration procedure have been proposed in literature to determine either the electrical properties, or both the electrical properties and thickness of various layers [4]-[11]. These techniques can be classified either as half space (reflection only), or the full reflection-transmission methods requiring access to both sides of the test medium.

It may be mentioned that most of the conventional time domain techniques proposed earlier for different applications such as ground penetrating radar, through-wall imaging fall under the category of the reflection only approach, where one doesn't have access to other side of the object and hence only the reflection data are employed in order to solve the corresponding inverse problem. Now, for these reflection based approaches, the data domain is limited and hence the inverse solution becomes quite sensitive to any change in the measured data. It is mainly due to this reason that the combined reflection-transmission approach is proposed in this work for the RF imaging of stationary and moving objects. The proposed scheme makes use of both reflection and transmission data in order to expand the data and observation domain thereby making the overall technique to be more rugged and robust in comparison to the reflection only method. The other issue with most of the earlier approaches has been the requirement of an additional reference measurement (in general a metal plate) for the actual calibration procedure [4]-[9]. However, the use of a metal plate as the reference standard does not look quite appropriate for real time imaging applications due to various reasons. The first problem is that the use of a metal plate as the reference standard requires the test object to be displaced from the original position, which does not look very convenient. In addition, the whole measurement procedure becomes position sensitive thereby indicating the possibility of error in the reconstruction if the test object is not properly aligned with respect to the interrogating sets of antennas. The last issue with currently available time domain imaging techniques has been that most of them use some form of iterative procedure which make them computationally expensive and hence limit their usage for real time applications.

In order to deal with the problems discussed above, a novel time domain reflection-transmission non-iterative RF imaging scheme, without requiring any reference calibration, was recently introduced [11]. However, in [11] only the theoretical results were provided to obtain 2D dielectric image of the test medium for the single layer lossless medium. The aim of this paper is to extend the overall applicability of the earlier proposed approach for multiple layers by combining the time domain technique with the Riccati equation based approach [16]-[17]. In addition, now the test medium is considered to be lossy and hence the permittivity as well as the effective conductivity of multiple layers is now reconstructed. More importantly, the experimental validation of the proposed approach is now carried out by reconstructing the RF image of various objects using a set of developed Vivaldi antenna arrays [18]-[20]. The fabricated antenna arrays are used to scan a human mannequin with the metal plate concealed behind the cloth in order to detect the presence of hidden objects. It is observed that if the mannequin is moved between the pair of antenna arrays, the

Z. Akhtar, A. K. Jha and M. J. Akhtar are with the Department of Electrical Engineering, Indian Institute of Technology Kanpur, Uttar Pradesh 208016, India (e-mail: zuakhter@iitk.ac.in, akjha.RF@gmail.com, mjakhtar@iitk.ac.in)
The authors acknowledge the support from the ISRO Space Technology Cell for funding a project with grant no. STC/EE/2015100.

measured scattering parameters at various positions can be used in conjunction with the proposed time domain imaging scheme to obtain the 2D image of the medium under test. The obtained 2D image can then be used to detect the presence of a metallic object hidden behind the scene. The proposed approach is quite useful for applications such as online monitoring of objects in industrial tomography, and for security applications to identify contraband detection, where one has access to both sides of the test area.

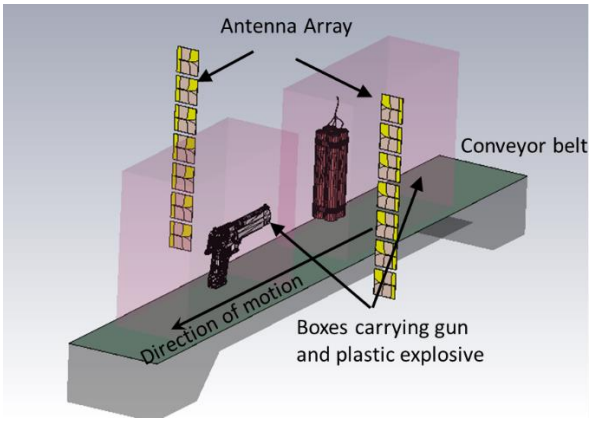

Fig. 1. Schematic illustration of the online time domain microwave imaging system

The overall manuscript is organized as follows. Section II provides a detailed explanation of the proposed theoretical algorithm in order to image the test medium in terms of the time domain scattering data. The numerical simulation along with some analysis is presented in Section III using the electromagnetic simulator, the CST studio. The prototype of the actual measurement setup including performance tests of the proposed technique are given in Section IV. In this section, the practical limitations of various parameters such as bandwidth and the antenna's directional characteristics affecting the image resolution are also described. Finally, the concluding remarks are given in Section V.

II. MICROWAVE IMAGING SCHEME

The microwave imaging procedure involves exciting the test medium with an electromagnetic wave of microwave range in order to measure the reflection and transmission data. The measurement is normally carried out using a vector network analyzer (VNA) and associated RF components. The measured reflection and transmission data are then used to retrieve the electromagnetic and structural properties of the test medium with the help of some inverse reconstruction algorithm. The proposed imaging system setup is shown in Fig.1, where the test objects with different spatial dielectric profile are assumed to be moving on the conveyor belt. The real time imaging and online monitoring of the test object is facilitated with the help of two antenna arrays and associated receiver and transmitter modules of the RF system as shown in this figure.

A. Problem formulation

Let us first consider the situation depicted in Fig. 2, where the multilayered test medium with relative permittivities $\varepsilon_{rt1},\varepsilon_{rt2},....\varepsilon_{rtN}$, effective conductivities $\sigma_{t1},\sigma_{t2},....\sigma_{tN}$ and corresponding thicknesses $d_{t1},d_{t2},....d_{tN}$ is placed in a lossless nondispersive background (air in present case) between the transmit/receive (TR) systems.

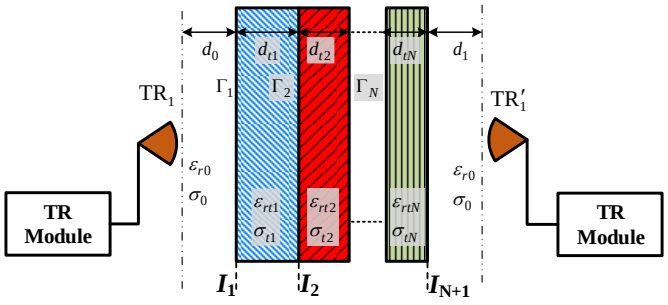

Fig. 2. Representation of the proposed RF imaging system

Without any loss of generality, let us assume the TR system to be excited with a current/ voltage pulse. The signal received by TR systems, either for the reflected or, for the transmitted wave can be expressed using the following expression

$$\aleph = \mathrm{P}_{inc}\sum_{k=1}^{\infty}\Upsilon_k\,\Re_k\,\mathrm{A}_k\,u\left(t-\tau_k\right) \tag{1}$$

The term Υ in the above expression refers to the actual propagation condition, which in the present situation corresponds to a plane EM wave incident normally over the test medium. The term $\Re$ represents the coefficient to take into account the reflection and transmission factor from different layers, whereas the term $\mathrm{A}_k = f\left(\sigma_t,\eta_0,d_t,\varepsilon_{rt}\right)$ considers the effect of absorption through the test medium corresponding to k^{th} reflection/transmission peak. The term $u(t)$ is the unit step function indicating the presence of the received waveform with τ representing the time of arrival of the received signal.

B. Reconstruction algorithm (single layer medium)

In this section, the procedure to evaluate the parameters of the medium under test (MUT), consisting of a single layer surrounded by the background medium from both sides, is presented. The evaluation is carried out in terms of the measured quantities i.e., $P_{r1},P_{r2},P_{t1},P_{t2}$ and their corresponding times of occurrence. The simplified bounce diagram shown in Fig. 3 represents the transmitted and reflected powers from the test medium in time domain. The TR_1 and TR_1' in this figure denote the transmit/receive RF modules on both sides of the interrogating medium, which are primarily responsible for the transmission and reception of the RF power.

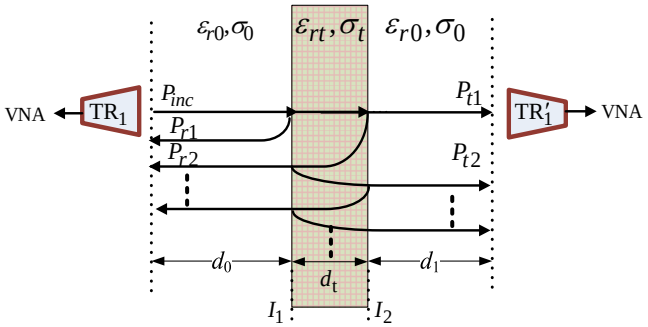

Fig. 3. A bounce diagram for the single layer medium with the incident wave experiencing infinite number of reflections and transmissions at both interfaces

The first reflected power peak from the front interface (I_1) recorded at TR_1 in Fig. 3 can be expressed as

$$P_{r1} \cong \Upsilon_1 \Re_1 \mathrm{A}_1 u(t-T_1) \mathrm{P}_{inc} \tag{2}$$

where, Υ_1 represents the two way path loss, $\Re_1$ signifies the reflection from the interface I_1, A_1 models the material absorption corresponding to first reflection peak and T_1 denotes the time of arrival corresponding to the first reflection peak. It is noted that the value of A_1 would be unity since we are assuming the background medium to be air.

In a similar way, the reflected power from the second interface can be expressed as

$$P_{r2} \cong \Upsilon_2 \Re_2 \mathrm{A}_2 u(t-T_2) \mathrm{P}_{inc} \tag{3}$$

where Υ_2 represents the two way path loss, $\Re_2$ includes the two transmission factors at interface I_1 and one reflection from the interface I_2, and T_2 denotes the time of arrival for the second peak as shown in Fig. 3.

On the other end, the direct transmitted component received at TR_1' can be expressed as

$$P_{t1} \cong \Upsilon_3 \Re_3 \mathrm{A}_3 u(t-T_3) \mathrm{P}_{inc} \tag{4}$$

where Υ_3 represents one way direct path loss, $\Re_3$ signifies the two transmission factors at interface I_1 and I_2 as shown in Fig. 3, and T_3 now denotes the arrival time of the first transmission peak. The second transmission peak can be expressed as

$$P_{t2} \cong \Upsilon_4 \Re_4 \mathrm{A}_4 u(t-T_4) \mathrm{P}_{inc} \tag{5}$$

where all the symbols have the usual meaning as described in earlier cases.

The transmission and reflection peaks relating the MUT parameters such as the dielectric constant, the effective conductivity, and thickness of the MUT can be derived to have the following closed forms if the plane wave propagation is assumed inside the test medium

$$P_{r1} \cong \Upsilon_1 |\Gamma_1|^2 \mathrm{P}_{inc} \tag{6}$$

$$P_{r2} \cong \Upsilon_2 |\Gamma_1|^2 (1-|\Gamma_1|^2)^2 \exp(-2\sigma_{t1}\eta_0 \frac{1}{\sqrt{\varepsilon_{rt1}}} d_{t1}) \mathrm{P}_{inc} \tag{7}$$

$$P_{t1} \cong \Upsilon_3 (1-|\Gamma_1|^2)^2 \exp(-\sigma_{t1}\eta_0 \frac{1}{\sqrt{\varepsilon_{rt1}}} d_{t1}) \mathrm{P}_{inc} \tag{8}$$

$$P_{t2} \cong \Upsilon_4 (1-|\Gamma_1|^2)^2 |\Gamma_1|^4 \exp(-3\sigma_{t1}\eta_0 \frac{1}{\sqrt{\varepsilon_{rt1}}} d_{t1}) \mathrm{P}_{inc} \tag{9}$$

where $\eta_0 = 377\ \Omega$ (free space intrinsic impedance). Since the waves representing P_{r1}, P_{r2} and P_{t1}, P_{t2} experience the same amount of path loss, it can be assumed that $\Upsilon_1 = \Upsilon_2$, and $\Upsilon_3 = \Upsilon_4$. Using this concept, and with the help of (6)-(9), the following relationship can be obtained

$$\left(\frac{P_{r1}}{P_{r2}}\right)\left(\frac{P_{t2}}{P_{t1}}\right) \equiv f(\Gamma_1) = \left(\frac{|\Gamma_1|^2}{(1-|\Gamma_1|^2)}\right)^2 \tag{10}$$

where Γ_1 is the reflection coefficient defined at interface I_1

$$\Gamma_1 = \frac{\bar{Z}_t - \bar{Z}_0}{\bar{Z}_t + \bar{Z}_0} = \frac{1/\sqrt{\varepsilon_{rt1}} - 1/\sqrt{\varepsilon_{r0}}}{1/\sqrt{\varepsilon_{rt1}} + 1/\sqrt{\varepsilon_{r0}}} = \frac{1-\sqrt{\varepsilon_{rt1}}}{1+\sqrt{\varepsilon_{rt1}}} \tag{11}$$

with $\bar{Z}_t$, $\bar{Z}_0$ representing the normalized characteristic impedances of the test medium and that of free space, respectively. As P_{r1}, P_{r2}, P_{t1} and P_{t2} represent directly measurable quantities, the reflection coefficient Γ_1 at interface I_1 can be easily obtained by solving (10) with the constraint $|\Gamma_1| < 1$. After computing the value of Γ_1, the permittivity, and thickness of the test medium can be determined with the help of following expressions

$$\varepsilon_{rt} = \varepsilon_{r0}\left(\frac{1+|\Gamma_1|}{1-|\Gamma_1|}\right)^2 \tag{12}$$

$$d_{t1} = \frac{c\,\Delta\tau_1}{2\sqrt{\varepsilon_{rt1}}} \tag{13}$$

$$\sigma_{t1} \cong \frac{1}{2d_{t1}}\sqrt{\frac{\varepsilon_0\varepsilon_{rt1}}{\mu_0}} \ln\left(\frac{P_{r1}}{P_{r2}}\left(1-|\Gamma_1|^2\right)^2\right) \tag{14}$$

where symbols c and μ_0 represent the velocity of light in vacuum and permeability of free space, respectively.

C. Reconstruction algorithm for multi-layered structure

In the previous section, the single layer medium was considered in order to explain the procedure of determining its dielectric constant, effective conductivity, and thickness using the proposed time domain procedure. However, the microwave imaging usually involves multilayered structure requiring reconstruction of each layer which is a challenging problem due to the presence of infinite multiple reflections. The problem of multiple reflections has recently been solved with the help of iterative procedures [7]-[8]. The imaging schemes based on the iterative procedures introduce computational complexity when the number of layers is increased beyond a certain limit.

The objective of this paper is to propose a multilayered non-iterative scheme, which can be considered as a combination of two techniques viz., the generalized time domain approach [8] and the Riccati reconstruction algorithm [16]. It is worth mentioning that both the individual reconstruction techniques i.e., [8], [16] have certain limitations in terms of accurate reconstruction of multilayered structure. The Riccati approach [16] is, for example, valid for a multilayered lossless medium whereas the generalized time domain technique [8] requires some priori information in order to reconstruct different layers of the test medium. The proposed reconstruction procedure takes the advantage of both techniques, which facilitates the reconstruction of the multilayered lossy medium with substantial accuracy without using any iterative procedure. The proposed approach can be itemized as follows

1) The scattering parameters are measured for the multilayered structure as depicted in Fig. 2.
2) The Riccati based reconstruction approach is applied on the modified (time-gated) reflection coefficient data i.e., S_{11} or $S_{22.}$
3) The permittivity profile information obtained with the help of Riccati based reconstruction is finally used in the generalized time domain approach to calculate the properties i.e., ε_{rt} , σ_t and d_t of various layers of the test medium.

The above points explain the overall procedure conceptually with the details being presented in subsequent sections in the later part of the paper. Now, in case of multilayered structure, the reflection from each interface can be expressed in similar manner as mentioned in (6) and (7). With reference to Fig. 2, various direct reflections received at TR_1 in this case can be expressed as

$$P_{r1} \equiv \left|\Gamma_1\right|^2 \mathrm{P}_{inc} \tag{15}$$

$$P_{r2} \equiv (1-\left|\Gamma_1\right|^2)^2 \left|\Gamma_2\right|^2 e^{-2\eta_0 \frac{\sigma_{t1} d_{t1}}{\sqrt{\varepsilon_{rt1}}}} \mathrm{P}_{inc} \tag{16}$$

$$P_{r3} \equiv \left\{(1-\left|\Gamma_1\right|^2)^2 (1-\left|\Gamma_2\right|^2)^2 \left|\Gamma_3\right|^2\right\} e^{-2\eta_0 \left(\frac{\sigma_{t1} d_{t1}}{\sqrt{\varepsilon_{rt1}}} + \frac{\sigma_{t2} d_{t2}}{\sqrt{\varepsilon_{rt2}}}\right)} \mathrm{P}_{inc} \tag{17}$$

$$P_{rN} \equiv \left\{(1-\left|\Gamma_1\right|^2)^2 (1-\left|\Gamma_2\right|^2)^2 .....\left|\Gamma_N\right|^2\right\} \times e^{-2\eta_0 \left(\frac{\sigma_{t1} d_{t1}}{\sqrt{\varepsilon_{rt1}}} + \frac{\sigma_{t2} d_{t2}}{\sqrt{\varepsilon_{rt2}}} + ... + \frac{\sigma_{t(N-1)} d_{t(N-1)}}{\sqrt{\varepsilon_{rt(N-1)}}}\right)} \mathrm{P}_{inc} \tag{18}$$

From (15) and (16), we have

$$\sigma_{t1} \equiv \frac{1}{2d_{t1}} \sqrt{\frac{\varepsilon_0 \varepsilon_{rt1}}{\mu_0}} \ln\left(\frac{P_{r1}}{P_{r2}} \times \frac{\left|\Gamma_2\right|^2 \left(1-\left|\Gamma_1\right|^2\right)^2}{\left|\Gamma_1\right|^2}\right) \tag{19}$$

It is evident from the above equation that (14) represents a special case of (19), when $\left|\Gamma_1\right| = \left|\Gamma_2\right|$, which can be a valid assumption in case of uniform background with plane wave propagation. In general, the effective conductivity of the N^{th} layer can be expressed as

$$\sigma_{tN} \equiv \frac{1}{2d_{tN}} \sqrt{\frac{\varepsilon_0 \varepsilon_{rtN}}{\mu_0}} \ln\left(\frac{P_{rN}}{P_{rN+1}} \times \frac{\left|\Gamma_{N+1}\right|^2 \left(1-\left|\Gamma_N\right|^2\right)^2}{\left|\Gamma_N\right|^2}\right) \tag{20}$$

From (15)-(18), it is evident that $P_{r1}, P_{r2}, .. P_{rN}$ are measurable quantities. It means that if the real permittivity profile of the multilayered medium is known or determined in advance, then it can be used to estimate the effective conductivity of individual layers. The initial value of the multilayered permittivity profile is obtained here using the Riccati reconstruction procedure with few modifications as given below in order to make it compatible with the free space measurement technique.

1) Firstly, the Riccati approach in the present situation is made applicable to band limited data so that approximate values of the dielectric constant and corresponding thickness of individual layers can be obtained [17].
2) The issue of assuming no reflection from infinity (matched end) in the conventional Riccati procedure is resolved using the standard time gating procedure.

The details of the modification required in the conventional Riccati procedure are described in the respective sections later in this paper. It should, however, be noted that the Riccati reconstruction procedure takes into account multiple reflections and concurrent reception, which are still bottlenecks for the conventional time domain methods [7], [8]. Therefore, the approach of combining the time domain method with the Riccati procedure is quite helpful. The flow diagram for the reconstruction of multilayered medium using the proposed scheme is shown in Fig. 4.

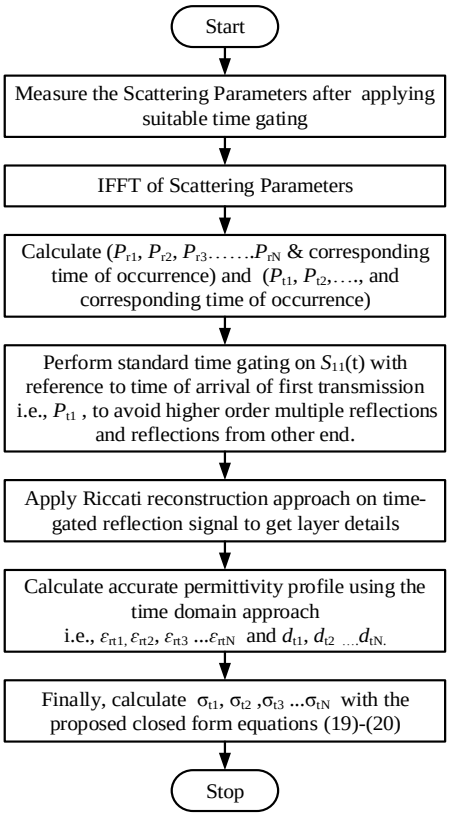

Fig. 4: Flow chart for the multilayered time domain reconstruction approach

It is noted that the scheme shown in Fig.4 represents a general case where the proposed time domain approach is combined with the Riccati based algorithm. This scheme is mainly applied for the multi-layered medium in order to obtain approximate permittivity values of different layers. The conventional Riccati approach usually requires the reflection coefficient data to be measured at a pre-defined reference plane.

D. Modification in Riccati reconstruction procedure

The Riccati reconstruction approach determined the sub-surface permittivity profile starting from the reference plane of

measurement. The closed form inverse solution of the Riccati equation is as follows [16]

$$\varepsilon_r(l) = \exp\left[-4\int_0^l \hat{r}(l')dl'\right] \tag{21}$$

where $l = 2\int_0^x \sqrt{\varepsilon_r(x')}\,dx'$, while $\hat{r}(l')$ represents inverse Fourier transform of renormalize reflection coefficient. The proposed approach assumes both the reflection and transmission data to be available, and hence the time domain and the Riccati equation approach can be employed wherever applicable. However, under the situation where a metal object appears in between the antenna pair leading to zero transmission, only the reflection data can be utilized. Now, this reflection data would correspond to the scenario where the test object is backed by a metal layer. Hence, this reflection data cannot directly be utilized in the conventional Riccati approach, which assumes a matched condition at the end. In order to facilitate the usage of Riccati approach for this metal backed situation to estimate the dielectric profile of the test medium, a number of simulations and measurements using various reference materials are carried out. It emerged that the lower half frequency band of the metal backed reflection data can be used in the Riccati approach after removing the reflection peaks corresponding to the metal plate through the standard time gating function. The modified reflection data can now be utilized in conjunction with the Riccati approach followed by the proposed time domain scheme to reconstruct the permittivity and conductivity profile of the test medium near to metal position. This approach can essentially be used from both the ends i.e., both S_{11} and S_{22} can be employed to retrieve the permittivity and conductivity profile from the two ends of the test medium.

The standard time gating function, which basically refers to removal of reflections beyond a point in the effective time domain, is used to achieve the matched condition at the end of the medium. However, the quality of reconstruction degrades with the modified boundary condition. Nevertheless, it is possible to fetch significant information such as boundaries of various layers in order to obtain a qualitative dielectric image of the medium under investigation. In order to see the effect of time gating in the Riccati procedure, a three layer medium is considered as shown in Fig. 5.

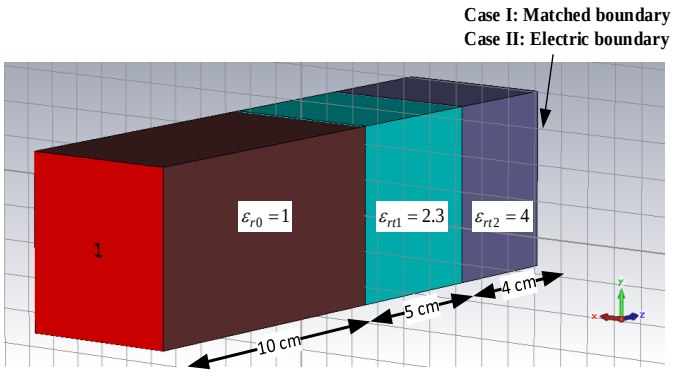

Fig. 5. Three layer medium considered to investigate the performance of time gating

The simulations are carried out in 0-40 GHz band for two different scenarios i.e., z_{max} boundary is considered to be matched for case I, while it is taken as PEC for case II. The proposed scheme basically tries to avoid reflections due to the PEC boundary and converts scattering parameters of case II equivalent to that of case I with the help of the standard time-gating and Fourier transform approach so that the Riccati procedure can be applied. The assessment of this improvement can be visualized with the help of Figs. 6 and 7 where the time gated transformed reflection coefficient is compared with the actual matched case. It can be observed from both the plots that the proposed gating scheme works quite well in the lower frequency range but the response gets slightly degraded in the higher frequency range.

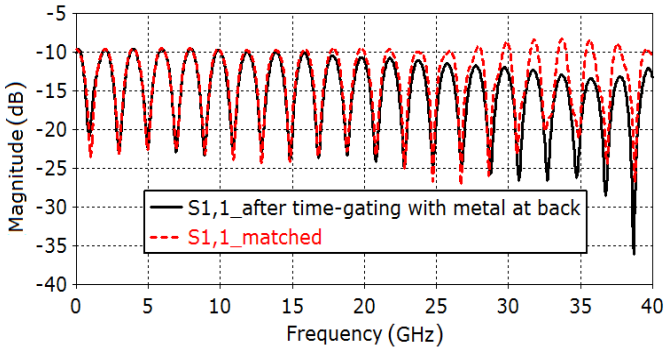

Fig. 6. Magnitude of reflection coefficient in case I and case-II

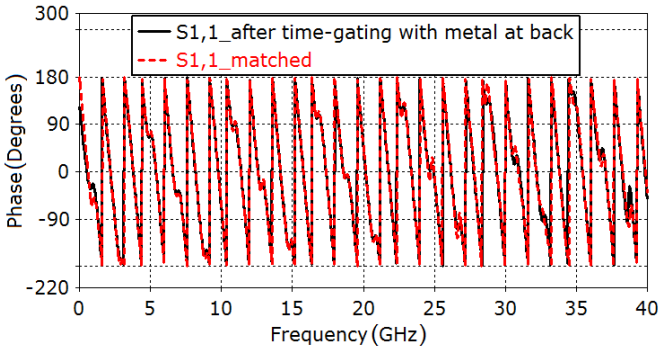

Fig. 7. Phase of reflection coefficient in case I and case II

III. Numerical Simulation and Sensitivity Analysis

CST microwave studio is mainly employed here for carrying out the simulation and performing the sensitivity analysis of the proposed approach. The applicability of the proposed scheme for a single layer lossless medium and for simple 2-D geometry has already been proposed earlier [11]. The full wave simulation of the test medium is usually carried out in order to calculate the *S*-parameters over the frequency range of 0-40 GHz. The symmetry plane reduction technique is used to reduce the numerical simulation time. A total of 5000 frequency samples and 1.86 M mesh cells are taken over the working frequency range for a typical single layer medium. The boundaries are chosen such that the plane wave assumption is valid. In order to obtain an idea about sensitivity of the proposed scheme, a detailed parametric analysis is performed here. However, the thickness of the dielectric sample is kept to be same, i.e., d_t =5 mm in all simulations. The simulated *S*-parameters are then used

to calculate various system variables (P_{r1}, P_{r2}, P_{t1} and P_{t2}) using the standard inverse Fourier transform technique to study their behavior with respect to system parameters i.e., ε_{rt}, σ_t and d_t. The typical time domain reflection power plots for the present situation are shown in Fig. 8, where a variation in primary and secondary reflection peaks by changing the dielectric properties of the test sample can be observed.

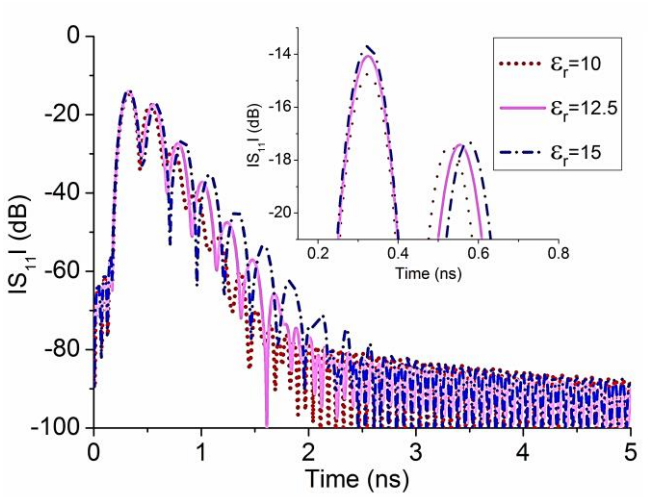

Fig. 8. Time domain reflection coefficient peaks P_{r1} and P_{r2} as relative permittivity varies from 10 to 15. ($\sigma_t = 0$, $d_t = 5$ mm)

A similar kind of primary and secondary transmission peaks can also be observed by plotting the transmission coefficient [11]. These simulated reflection and transmission curves can then be used to plot the reflection and transmission power with respect to the material electrical conductivity as shown in Fig. 9. It can be observed from this figure that the value of P_{r1} is almost independent of conductivity for these range of material parameters, while the power term P_{t2} is very sensitive to the material conductivity. The terms P_{r2} and P_{t1} change slightly over the range indicated.

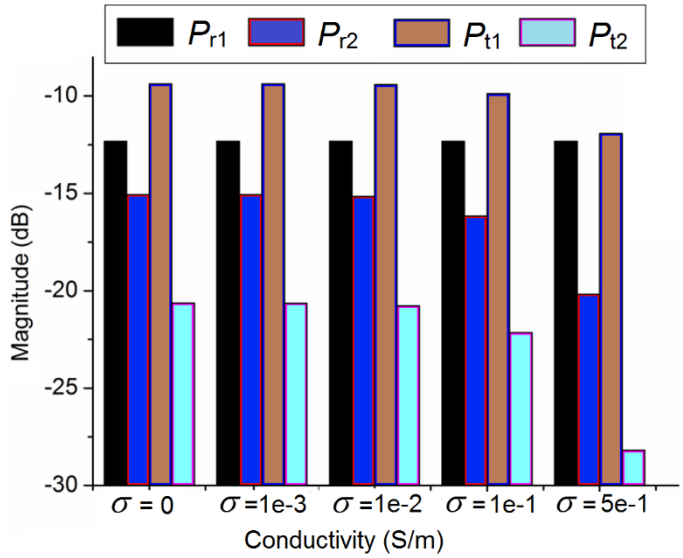

Fig. 9. Variation in reflection and transmission power peaks when the effective electrical conductivity varies from 0 to 0.5

IV. MEASUREMENT RESULTS AND DISCUSSION

A. Antenna array design for the imaging system

Two antenna arrays based on Vivaldi structure are designed for validating the concept of proposed scheme. The primary reason for choosing the Vivaldi antenna as the basic element in the present situation is due to the fact that it exhibits ultra-wide band characteristics. The detailed design procedure and parameters of the antenna element can be found in [19]-[20]. The two designed arrays, with each array consisting of 7 antennas, are displayed in Fig. 10. It can be observed from this figure that the individual antenna elements in each array are placed at a uniform distance. The antenna support frame is made of acrylic having one degree of freedom in order to adjust the separation between the arrays. The antennas in each array are placed at spacing of 10 cm with alternate orthogonal polarization as shown in figure below.

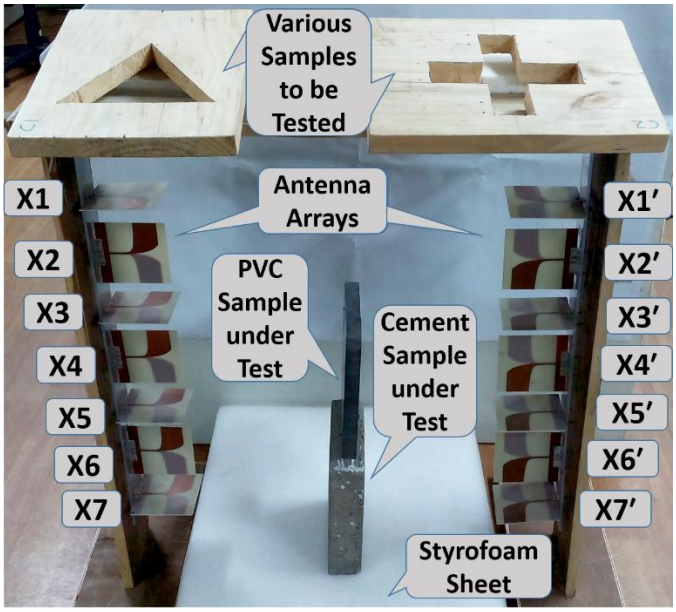

Fig. 10. Fabricated prototype antenna array with alternate orthogonal polarization

The mutual coupling between the individual elements is minimized in the present situation using the alternate orthogonal polarization, which is crucial in order to design an efficient antenna array. The mutual coupling can be quantified in terms of isolation between antenna elements, which should be quite high since the poor isolation might degrade the actual received signal. The isolation between individual elements of the proposed antenna system is obtained by measuring the transmission coefficient between two neighboring antennas of the actual fabricated array shown in Fig. 10. The measured transmission data between elements X3 and X4, and between X5 and X4 of the fabricated array, with the two neighboring elements having orthogonal polarization, is shown in Fig. 11. From Fig. 11, it can be noted that the isolation between the neighboring antenna elements of the proposed array is of the order of 30 dB in the lower frequency range, which goes up to 45 dB in the higher frequency range. As the antenna elements used in the present setup are always having alternate orthogonal polarization, the performance of any antenna is not significantly affected due to the presence of neighboring antennas.

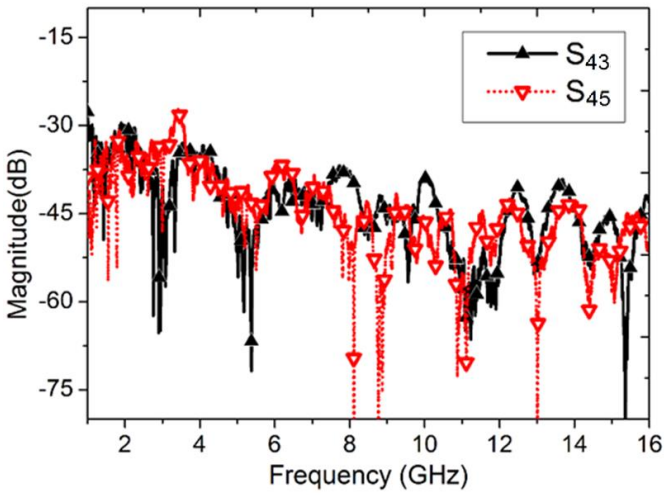

Fig. 11. Measured isolation between the antenna elements in proposed configuration i.e., alternate orthogonal polarization

The actual measurement setup for the imaging is shown in Fig. 12, which consists of a vector network analyzer, the designed antenna arrays, and automated *xy* scanner. This scanner supports the two dimensional movement with a minimum step of 0.5 mm. The stepper motors drives are controlled by an open source computing platform i.e., Arduino platform. A LabVIEW program is developed for interfacing the VNA with the *xy* scanner which facilitates the automated recording of *S*-parameters at each point. The measured *S*-parameters are then used to image the test medium using the proposed scheme.

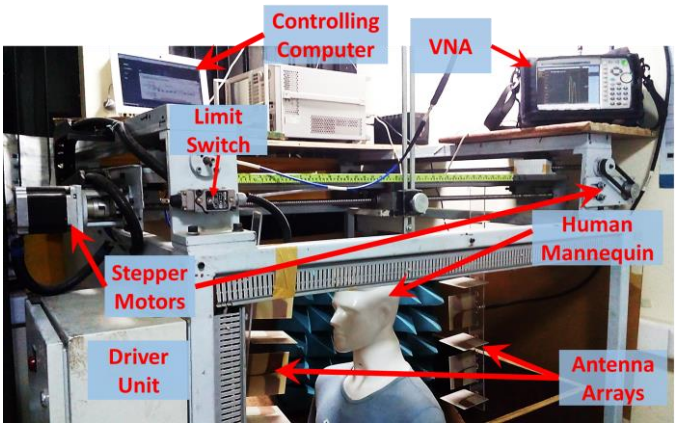

Fig. 12. Actual automated scanning measurement setup

B. Image resolution and bandwidth requirements

The bandwidth and directional characteristics of the antenna/sensor play quite important role in achieving RF images of the test medium with enhanced resolution. As the proposed approach is bi-static, hence the resolution of the image depends quite strongly on bandwidth and directional characteristics of the antenna as compared to the multistatic approaches [21] where a synthetic aperture can play a significant role to enhance the image resolution. However, the proposed scheme can also be used in the multistatic configuration with additional computational cost. In general, the resolution of a typical 3D microwave image can be classified into two categories viz. the spatial and the axial. The spatial resolution also known as the lateral resolution depends on the operating frequency and directional characteristics of the antenna using the following expression [21]

$$\delta_{xy} \approx \frac{\lambda}{D_{xy}} L \tag{22}$$

where λ is the wavelength, $D_{x,y}$ represents the aperture along the lateral direction, and L is the distance between object and aperture. The axial resolution, δ_z along the depth is mainly determined by the signal bandwidth of the measured scattering data as follows [21].

$$\delta_z \approx \frac{c}{2 \times BW} \tag{23}$$

The bandwidth is a very crucial parameter in order to increase the resolution of the obtained RF image along the depth. Actually, the large signal bandwidth leads to an equivalent shorter pulse duration thus providing a high value of axial resolution. A minimum value of bandwidth is usually required in order to distinguish two thin adjoining layers of the stratified medium having distinct dielectric properties. In general, the RF image of the test medium with a good axial and lateral resolution can be obtained using the ultra-wide band (UWB) antennas with high directivity.

C. Measurement setup and imaging results

The simple medium with two interfaces is realized using the air-dielectric-air configuration as shown in Fig. 3, where various standard samples are placed at the dielectric position in order to validate the proposed algorithm in quantitative terms. Each standard dielectric sample (Acrylic, PMMC, PVC and Teflon) is having dimension of 20 cm × 25 cm × 2.5 cm, whereas the wooden, and cement based samples are having dimensions of 40 cm × 30 cm × 3 cm and 20 cm × 25 cm × 6.5 cm, respectively. The measured scattering data are transformed into the time domain with the help of inverse Fourier transform so that various transmission and reflection peaks can be determined. By applying the proposed algorithm, the permittivity, conductivity, and thickness of the MUT have been calculated. The calculated parameters are also shown in Fig. 13.

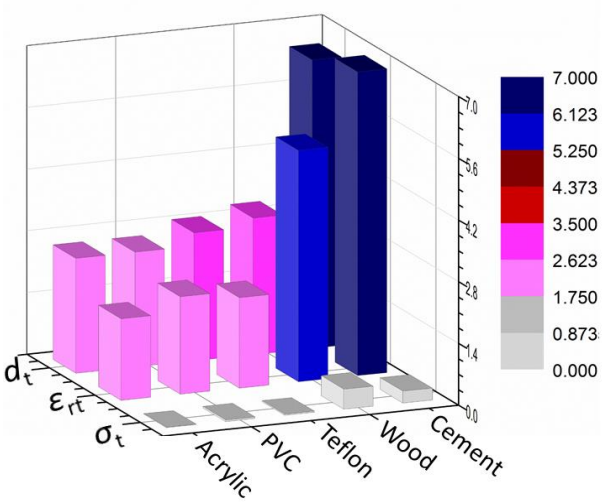

Fig. 13. Measured values of dielectric constant, effective conductivity and thickness of various MUTs for configuration shown in Fig. 10

It is evident that, the applicability of the proposed algorithm directly depends on the identification of various reflection and transmission peaks as shown in Table I.

Table I. DIFFERENT CONDITIONS BASED ON THE DETECTION OF VARIOUS PRIMARY AND SECONDARY POWER PEAKS FOR SINGLE SLAB

Case	Characteristics of medium under test	P_{r1}	P_{r2}	P_{t1}	P_{t2}
1	No object or medium	×	×	√	×
2	Metal object	√	×	×	×
3	Dielectric object or medium	√	√	√	√

For example, case 1 in Table I corresponds to the situation when no medium is present between the measuring antenna elements, and hence no reflection peaks would be observed as there is no discontinuity present in the system. However, the primary transmission peak is successfully detected with a maximum power level. Similarly, case 2 indicates the state when there is a metal object obstructing the reception of electromagnetic radiation between the antennas, and hence maximum primary reflection is observed in this case. Lastly, case 3 shows the ideal situation, where all the power peaks are noticeable, and the proposed algorithm can directly be implemented. The applicability of the proposed scheme to image the dielectric medium along the lateral direction is investigated using the measurement configuration shown in Fig. 14, where M1, M2, and M3 represent distinct samples of non-homogeneous dielectric medium.

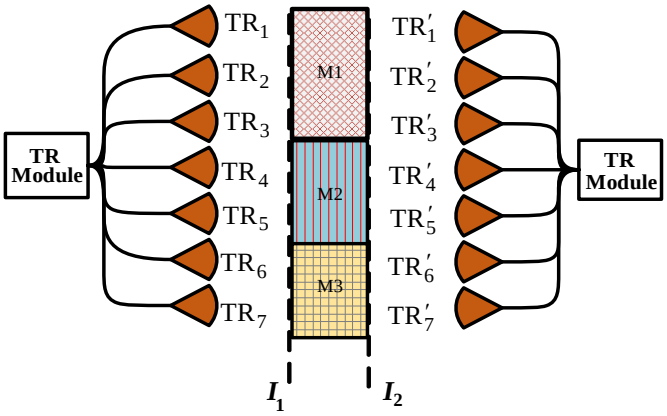

Fig. 14. Configuration for investigating the various material parameters in lateral direction

In this configuration, various samples are positioned in such a way that the electromagnetic wave is incident normally over the test medium. The relative permittivity, effective conductivity, and thickness are then calculated at each sampling location of the test medium. Different samples are placed at positions M1, M2, and M3 such that M1 occupies X1-X3, M2 occupies X4-X5, and M3 occupies X6-X7 as illustrated in Fig. 14 in order to realize the non-homogeneous structure. The practical realization of this configuration is shown in Fig. 10, where MUT is placed between the pair of antenna arrays corresponding to X1-X7 and X1′-X7′. The obtained values of relative permittivity, effective conductivity, and thickness of MUT calculated using (12)-(14) are plotted with reference to the lateral position i.e., X1, X2….X7 as shown in Figs. 15 and 16.

From Figs. 15 and 16, it can be observed that at location X1 to X3, the electromagnetic wave does not observe any discontinuity between the corresponding antenna pair (case 1 in Table I). Therefore, the values of relative permittivity and effective conductivity will be the same as that of the background medium (presently air). However, the thickness of the medium is calculated with the help of time of occurrence of primary transmission peak and gating start time.

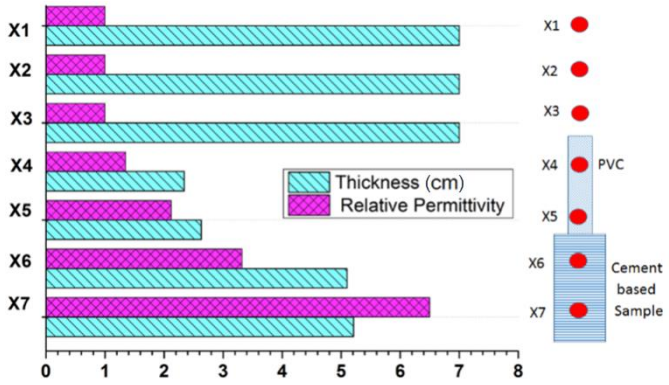

Fig. 15. The variation in relative permittivity and thickness along the lateral direction for the configuration shown in Fig. 14

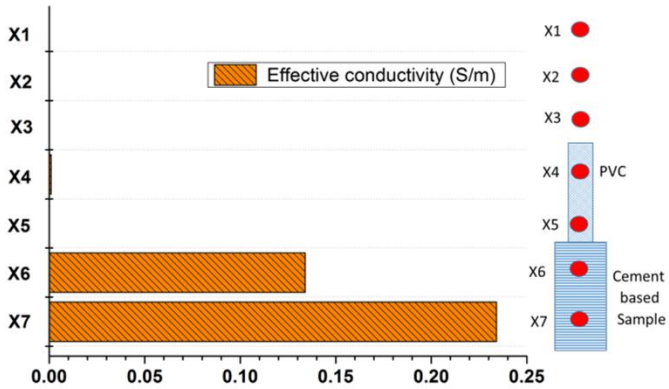

Fig. 16. The variation in effective conductivity along the lateral direction for configuration shown in Fig. 14

In the next step, the designed antenna array along with the proposed imaging scheme is used to obtain the 2D microwave image of a human mannequin with a concealed metallic object as shown in Fig. 17(a). The positions of all antenna elements along the mannequin are shown by X1, X2….X7. The test object in this case is moved between the two antenna arrays and 22 measurements along the horizontal direction are taken. The present case simulates the condition described as case 2 of Table I. It is noted that when antenna pair at X6 experiences a metal plate, its transmission power level drops to the noise floor of the measurement system. However, at other locations such as X1-X5 and X7, there will be some transmission. The primary transmission power peak is measured along various sampling locations. It is noted that the number of sampling points for this configuration is increased by a factor of 2 (14 vertical sampling points) to have sufficient resolution. This is facilitated by shifting each element of the designed array vertically by a

distance of 5 cm for taking another set of measurements by maintaining the test object at its position. Hence, the scattering measurements along the lateral plane of the test mannequin are carried out at 308 different locations. In order to smoothen the obtained image, the existing matrix consisting of a 14×22 set of measured data is resized with a factor of 10 using *imresize* function of Matlab. The resized matrix is then plotted with the help of the command *imagesc* of Matlab as shown in Fig. 17 (b). It can be observed here that the presence of the metallic object concealed inside the jacket can be detected and located correctly using the proposed imaging methodology.

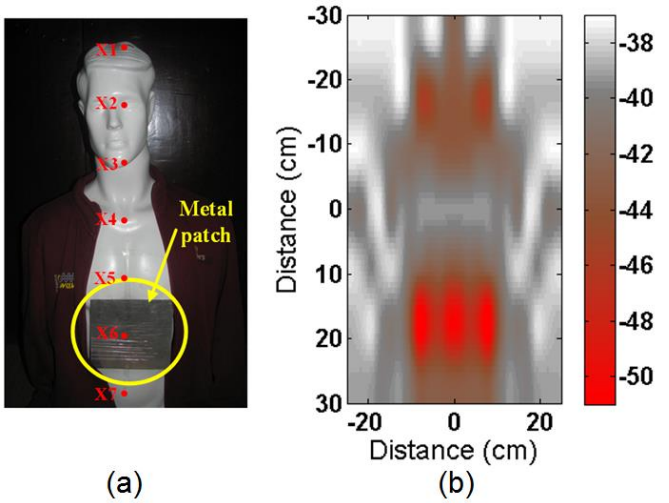

Fig. 17. (a) The human mannequin with concealed metallic patch considered for imaging (b) The corresponding transmissivity image obtained

After measuring the human mannequin, different shapes of wooden samples of semi dry chir pine (about 30 mm thick) are taken as shown in Fig. 18. These samples are placed in the imaging domain with the help of a sample holder. The scattering parameter measurements along the lateral plane of the test samples are carried out at different locations. The dielectric permittivity and effective conductivity at each sampling point are calculated with the help of proposed methodology. The images of these two samples after smoothening the data representing 14×24 measurements sets are shown in Figs. 19 and 20. It can be observed from Figs. 19 and 20 that the wooden samples can be distinguished from the background medium due to variation in the permittivity and conductivity values.

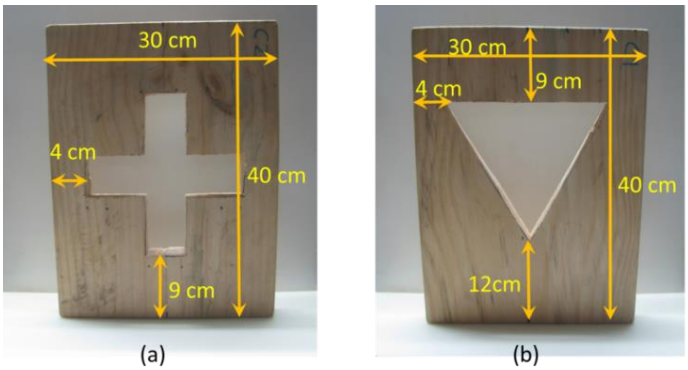

Fig. 18. The semi dry chir wooden sample with different type of shapes (a) red-cross symbol cut away from wooden slab (b) triangle cut away from wooden slab

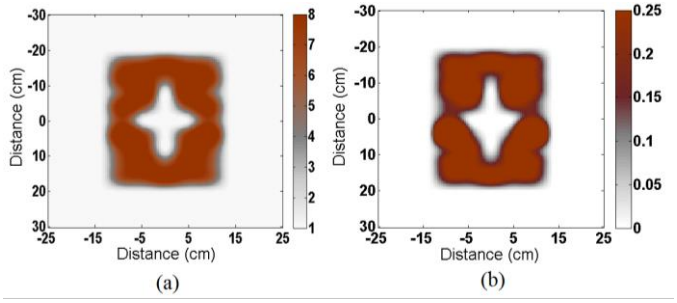

Fig. 19. 2D reconstructed images corresponding to the red-cross symbol (a) 2D permittivity image (b) 2D conductivity image, corresponding to the sample shown in Fig 18 (a)

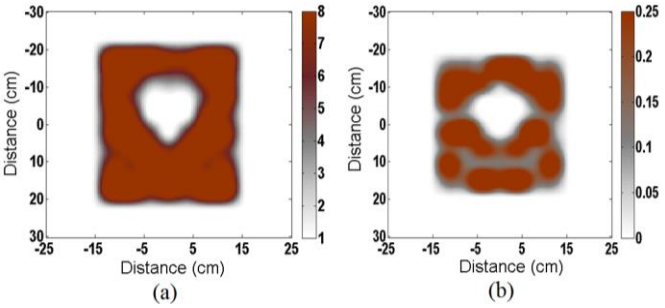

Fig. 20. 2D reconstructed images corresponding to the triangle symbol (a) 2D permittivity image (b) 2D conductivity image, corresponding to the sample shown in Fig 18(b)

Finally, a situation corresponding to the transmission zero condition is considered where the modified Riccati approach is first applied to obtain the permittivity profile of the stratified medium. The actual measured configuration considered for this situation is shown in Fig. 21, where a metal plate is placed at the extreme right hand side in order to show the applicability of the proposed reconstruction scheme based on the modified Riccati approach.

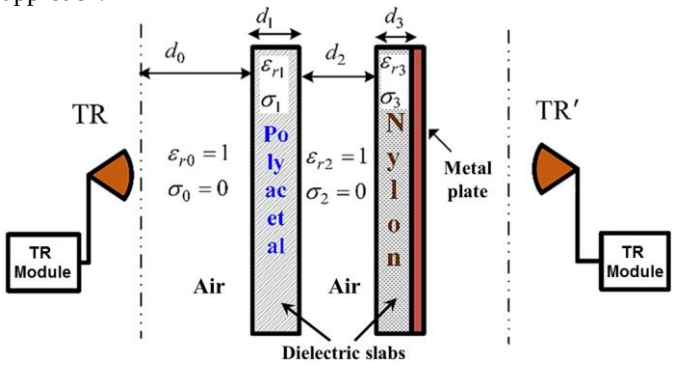

Fig. 21. The multi-layered (Air-Polyacetal-Air-Nylon-Metal-Air) imaging configuration with the metal plate placed at the end [$d_0 = 28$ cm, $d_1 = 30$ mm $d_2 = 70$ mm, and $d_3 = 30$ mm]

The reconstructed permittivity profile corresponding to the configuration shown in Fig. 21, is shown in Fig. 22. From this figure, it is evident that the modified Riccati approach is able to reconstruct the relative permittivity of Air-Polyacetal-Air layers of the multilayered medium with a reasonable amount of accuracy. However, the Nylon layer present near the metal layer cannot be accurately reconstructed due to limitation of the Riccati approach in the presence of a very sharp discontinuity as evident from Fig. 22.

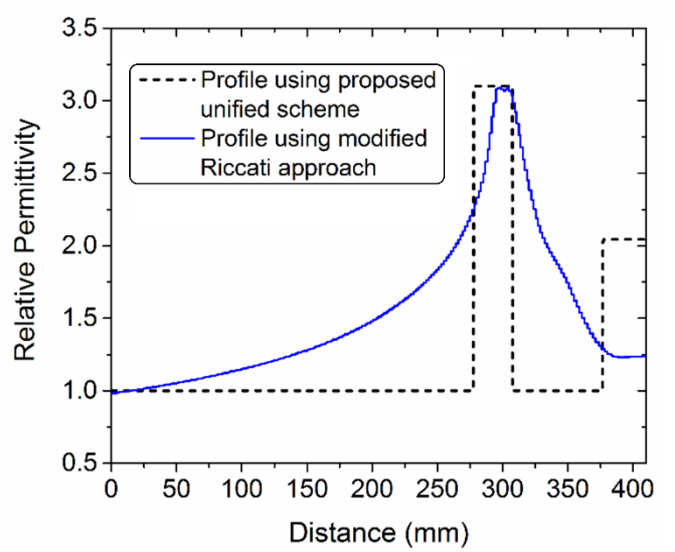

Fig. 22. Comparison reconstructed permittivity profile using modified Riccati approach with the proposed unified scheme for the multilayered (Air-Polyacetal-Air-Nylon) configuration shown in Fig 21

It should be noted that this kind of problem in reconstructing a sharp discontinuity generally occurs due to limited bandwidth of the measured reflection coefficient in the spectral domain. The problem becomes more severe in the present situation due to the presence of a metal plate at the end which reduces the effective bandwidth by almost half. For determining the thickness of various layers under limited bandwidth condition, a simple rule is applied where the geometric mean of permittivity of two adjacent layers is taken and the distance corresponding to this permittivity value is considered as the interface point. It should, however, be noted that the modified Riccati approach in the present situation is used to obtain approximate values of the permittivity only. The reconstructed permittivity data are then used as the initial guess for the proposed time domain approach to obtain the actual permittivity values and thicknesses of various layers. For the configuration shown in Fig. 21, various reflection peaks in the equivalent time domain received at TR1 are measured as $P_{r1} = -33.53$ dB, $P_{r2} = -39.78$ dB and $P_{r3} = -43.96$ dB corresponding to 2.33 ns, 2.68 ns and 3.14 ns, respectively. The gating start time i.e., t_{gs} for this situation is taken as 1.404 ns. The proposed time domain algorithm in this case successfully retrieves the relative permittivity of different layers as ($\varepsilon_{r0} = 1$, $\varepsilon_{r1} = 3.1$, $\varepsilon_{r2} = 1$ and $\varepsilon_{r3} = 2.045$), the effective conductivity as ($\sigma_0 = 0$, $\sigma_1 = 0.099$, $\sigma_2 = 0$) and thickness as ($d_0 = 27.78$ cm, $d_1 = 29.81$ mm, $d_2 = 69$ mm). The permittivity profile of the multi-layered media obtained using the time domain approach is plotted in Fig. 22, where it can be observed that permittivity of the Nylon layer can now be determined which could not be retrieved using the Riccati approach. However, the effective conductivity and thickness of the Nylon layer could still not be evaluated using the proposed scheme as this layer is directly in contact with metal, and the reflection peak corresponding to the metal is removed from the measured scattering data using the standard time gating procedure.

V. Conclusion

An attractive time domain RF imaging scheme has been presented to obtain 2D microwave images of various test objects. The proposed scheme successfully combines the conventional Riccati procedure with the time domain approach in order to obtain various layers of the stratified medium. The applicability of the approach for obtaining 2D dielectric and conductivity images have been shown by designing a pair of antenna arrays and employing them to scan the test medium containing some hidden objects. The validation of the proposed scheme has been carried out using both simulated as well as measured data, and is found to work for both stationary and moving objects. The proposed imaging technology has huge potential for security application where online monitoring and screening of moving objects over the conveyor belts can be facilitated to detect various explosives including unwanted arms and ammunitions using microwaves.

References

[1] A. M. Nicolson and G. F. Ross, "Measurement of the intrinsic properties of materials by time-domain techniques," *IEEE Trans. Instrum. Meas.*, vol. 19, no. 4, pp. 377-382, Nov. 1970.

[2] C. C. Courtney and W. Motil, "One-port time-domain measurement of the approximate permittivity and permeability of materials," *IEEE Trans. Microw. Theory Techn.*, vol. 47, no. 5, pp. 551-555, May 1999.

[3] B. K. Barman, Z. Akhter, M. J. Akhtar and S. Mishra, "Microwave nondestructive testing of cement based materials," *IEEE MTT-S International Microwave and RF Conference*, pp. 1-3, Dec. 14-16, 2013.

[4] S. L. Gupta, Z. Akhter, M. Bhaskar and M. J. Akhtar, "A novel half space time-domain measurement technique for one-dimensional microwave imaging," *83rd ARFTG Microwave Measurement Conference (ARFTG)*, pp. 1-4, Jun. 6, 2014.

[5] S. L. Gupta, Z. Akhter, M. Bhaskar and M. J. Akhtar, "Qualitative analysis of moisture content in cement based material using microwave non-destructive testing," *IEEE International Symposium on Antennas and Propagation Society*, pp. 924-925, Jul. 6-11, 2014.

[6] S. Caorsi and M. Stasolla, "Characterization of lossy layers through monostatic radar measurements," *13th Mediterranean Microwave Symposium* (MMS), pp. 1-4, Sept. 2-5, 2013.

[7] S. Caorsi and M. Stasolla, "A layer stripping approach for EM reconstruction of stratified media," *IEEE Trans. Geosci. Remote Sens.*, vol. 52, no. 9, pp.5855-5869, Sept. 2014.

[8] Z. Akhter and M. J. Akhtar, "Time domain microwave technique for dielectric imaging of multilayered media," *Journal of Electromagnetic waves and application*, vol. 29, no. 3, pp. 386-401, Jan. 2015.

[9] K. K. M. Chan, A. E.-C. Tan, L. Lin and K. Rambabu, "Material characterization of arbitrarily shaped dielectrics based on reflected pulse characteristics," *IEEE Trans. Microw. Theory Techn.*, vol. 63, no. 5, pp. 1700-1709, May 2015.

[10] S. P. Singh, Z. Akhter and M. J. Akhtar, "Calibration independent estimation of optical constants using terahertz time-domain spectroscopy," *Microw. Opt. Technol. Lett.*, vol. 57, pp. 1861–1864, 2015.

[11] Z. Akhter and M. J. Akhtar, "Online monitoring of moving objects on conveyor belt using RF time domain imaging technique," *IEEE MTT-S International Microwave and RF Conference*, pp. 1-3, Dec. 10-12, 2015.

[12] Z. Akhter and M. J. Akhtar, "Free-space time domain position insensitive technique for simultaneous measurement of complex permittivity and thickness of lossy dielectric samples," *IEEE Trans. Instrum. Meas.*, vol. 65, no. 10, pp. 2394-2405, Oct. 2016.

[13] B. J. Mohammed, K. S. Bialkowski and A. M. Abbosh, "Radar-based time-domain head imaging using database of effective dielectric constant," *Electronics Letters*, vol. 51, no. 20, pp. 1574-1576, Oct. 8, 2015.

[14] D. Byrne and I. J. Craddock, "Time-domain wideband adaptive beamforming for radar breast imaging," *IEEE Trans. Antennas Propag.*, vol. 63, no. 4, pp. 1725-1735, April 2015.

[15] Xu Li, S. K. Davis, S. C. Hagness , D. W. Van Der Weide and B. D. Van Veen, "Microwave imaging via space-time beamforming: experimental investigation of tumor detection in multilayer breast phantoms," *IEEE Trans. Microw. Theory Techn.*, vol. 52, no. 8, pp. 1856-1865, Aug. 2004.

[16] M. J. Akhtar and A. S. Omar, "Reconstructing permittivity profiles using integral transforms and improved renormalization techniques," *IEEE Trans. Microw. Theory Techn*., vol. 48, no. 8, pp. 1385-1393, Aug 2000.

[17] A. Kumar and M. J. Akhtar, "Microwave imaging of stratified media from band-limited reflection coefficient data," *IEEE Geosci. Remote Sens. Lett.*, vol. 11, no. 7, pp. 1255-1259, July 2014.

[18] P. Kumar, Z. Akhter, A. K. Jha and M. J. Akhtar, "Directivity enhancement of double slot Vivaldi antenna using anisotropic zero-index metamaterials," *IEEE Antennas and Propagation Society International Symposium (APSURSI)*, pp. 2333-2334, 2015.

[19] B. N. Abhijith and M. J. Akhtar, "Optimization of Vivaldi antenna for microwave imaging applications," *IEEE Antennas and Propagation Society International Symposium (APSURSI)*, pp. 1596-1597, July 6-11, 2014.

[20] Z. Akhter, B. N. Abhijeet and M. J. Akhtar, "Hemisphere lens loaded Vivaldi antenna for microwave imaging of concealed objects," *J. Electromagn. Waves App.*, vol. 30, no. 9, May 31, 2016.

[21] S. S. Ahmed, A. Schiessl, F. Gumbmann, M. Tiebout, S. Methfessel and L. Schmidt, "Advanced microwave imaging," *IEEE Microw. Mag*., vol. 13, no. 6, pp. 26-43, Sept.-Oct., 2012.

Zubair Akhter (S'13) received the bachelor's degree in electronics and instrumentation engineering from Anand Engineering College Agra, India, and the M.Tech. degree in RF and microwave engineering from IIT Roorkee, India in 2008 and 2011, respectively. He is currently pursuing the Ph.D. degree in electrical engineering with IIT Kanpur (IITK), India with a focus on microwave imaging, material characterization, non-destructive testing of materials, through wall imaging and ultra wide antennas for imaging applications.

He is currently involved in cost-effective solutions for microwave imaging of concealed objects, especially for homeland security applications. He has authored or co-authored over 23 scientific contributions published in peer-reviewed journals and various admired international conferences. His current research interests include developing a cost-effective microwave and millimeter wave imaging setup for real-time imaging of concealed object where objects can be classified on the basis of their dielectric signatures rather that its physical parameters, such as shape, and size.

Mr. Akhter is the Founder and a Chair of the IEEE Antennas and Propagation Society Student Branch Chapter IITK, Uttar Pradesh Section, India.

Abhishek Kumar Jha (S'14–M'17) received the B.E and M.Tech (Hons.) degrees in electronics and communication engineering from the University of Burdwan, West Bengal, India, in 2009 and 2011, respectively. He is a doctoral candidate in electrical engineering department of Indian Institute of Technology Kanpur (IITK), Kanpur, India. His research interests encompass the numerical analysis and design of microwave circuits and waveguide components, development of microwave sensors for nondestructive testing of dielectric and magnetic properties of materials, synthesis of advance composites for microwave absorbers and microwave heating applications, ENZ and MNZ sensors and devices etc. He has authored/coauthored approximately 30 papers in peer reviewed international journals and conference proceedings.

Mr. Jha founded and chaired the IEEE Microwave Theory and Techniques Society Student Branch Chapter IITK, Uttar Pradesh Section, India. He was a Project Trainee with the Microwave Tube Research and Development Centre, Defense Research and Development Organization, New Delhi, India, where he was involved in medium power injection locked magnetron. He was an Assistant Professor with the Electronics & Communication Engineering Department, Seacom Engineering College, Howrah, India, from 2011 to 2012. Mr. Jha is the recipient of various prestigious awards including BIRAC-GYTI and Microwave Graduate Fellowship in recognition of his academic achievement and excellence. He is also the recipient of the University Gold Medal for being first in the first class of B.E and M.Tech degrees in 2009 and 2011, respectively.

Mohammad Jaleel Akhtar (S'99–M'03–SM'09) received the Ph.D. and Dr. Ing. degrees in electrical engineering from the Otto-von-Guericke University of Magdeburg, Magdeburg, Germany, in 2003.

He was a Scientist with the Central Electronics Engineering Research Institute, Pilani, India, from 1994 to 1997, where he was involved in the design and development of high power microwave tubes. From 2003 to 2009, he was a Post-Doctoral Research Scientist and a Project Leader with the Institute for Pulsed Power and Microwave Technology, Karlsruhe Institute of Technology, Karlsruhe, Germany, where he was involved in a number of projects in the field of microwave material processing. In 2009, he joined the Department of Electrical Engineering, IIT Kanpur, Kanpur, India, where he is currently an Associate Professor. He has authored two books, two book chapters, and has authored or co-authored over 100 papers in various peer-reviewed international journals and conference proceedings. He holds one patent on coplanar based RF sensors. His current research interests include RF, microwave and THz imaging, microwave nondestructive testing, RF sensors, functional materials, wideband electromagnetic absorbers, UWB antennas for imaging, and design of RF filters and components using the electromagnetic inverse scattering.

Dr. Akhtar is a fellow of the Institution of Electronics and Telecommunication Engineers, New Delhi, India, and a Life Member of the Indian Physics Association and the Indo-French Technical Association. He is a recipient of the CST University Publication Award in 2009 from the CST AG, Darmstadt, Germany. He served as a Chair of the IEEE Microwave Theory and Techniques Society-S Uttar Pradesh Chapter from 2013 to 2015, and the Vice-Chair of the IEEE Uttar Pradesh Section in 2015.Uttar Pradesh Chapter, and Vice-Chair of the IEEE Uttar Pradesh Section.